Jpn. J. Appl. Phys. Vol. 42 (2003) pp. 5195–5199
Part 1, No. 8, August 2003

Determination of Mean-Field Coefficients of Ferroelectric Liquid Crystals

Jong-Wook JUNG, Sin-Doo LEE[1] and Jae-Hoon KIM*

Department of Physics, Hallym University, Chunchon, Kangwon-Do 200-702, Korea
[1]*School of Electrical Engineering, Seoul National University, P. O. Box 34, Kwanak, Seoul 151-742, Korea*

(Received January 8, 2003; accepted for publication April 10, 2003)

We studied phase transition from Sm A to Sm C* by the simultaneous measurements of tilt angle, dielectric constant, and pyroelectric coefficient as functions of temperature with various applied voltages. For ferroelectric liquid crystals with small electroclinic effect, the pyroelectric coefficients are maximum at the phase transition temperature, which does not depend on the applied voltage. However, for the maximum dielectric constant, temperature increases with increasing applied voltage. The difference from the transition temperature is proportional to $E^{2/3}$. Non-chiral Landau coefficients can be calculated from experimental results and compared with other results in the literature. [DOI: 10.1143/JJAP.42.5195]

KEYWORDS: ferroelectric liquid crystal, mean-field coefficient

1. Introduction

Since the discovery of ferroelectricity in tilted chiral smectic phases by Meyer,[1)] particularly, in the smectic C* (Sm C*) phase, ferroelectric liquid crystals (FLCs) have attracted considerable interest from fundamental as well as practical points of view.[2,3)] The surface stabilized FLC structure is demonstrated by Clark and Lagerwall.[2)] It is a suppression of the helicoidal twist of the Sm C* phase by surface forces. Since the structure can be operated in a bistable manner, numerous efforts in experiment and theory have been conducted for the understanding of the optical and electrical properties of the structure and its switching dynamics in external fields because of its potential application to flat-panel displays.[3)]

However, only a few attempts have been made to determine Landau expansion coefficient, which is important in correlating experimental results with theoretical description and in studying structural properties of FLCs.[4–9)] Particularly, non-chiral coefficients play an essential role in understanding the thermodynamic properties of the Sm C* phase because their contribution to the total free energy density describing an Sm A–Sm C* phase transition is much larger than that of chiral ones. Non-chiral coefficients have been obtained by sophisticated heat capacity measurements,[4,5)] or tilt angle, spontaneous polarization, and helical pitch measurements.[6,8,9)] Since Sm A and Sm C* liquid crystal phases are orientationally ordered fluids with a one-dimensional density wave, the simultaneous measurements of material parameters, such as tilt angle, spontaneous polarization, and dielectric constant, are essential to the precise determination of non-chiral coefficients. In this work, we study Sm A–Sm C* phase transition by the simultaneous measurements of tilt angle, dielectric constant, and pyroelectric coefficient, and determine non-chiral Landau expansion coefficients based on the experimental results.

2. Theory

In surface stabilized geometry with an external electric field, the classical Landau expansion can be written as

$$F = \frac{1}{2}a\theta^2 + \frac{1}{4}b\theta^4 + \frac{1}{2\chi}P^2 + CP\theta - PE. \tag{1}$$

The coefficient $a = \alpha(T - T_c)$ is temperature-dependent, whereas all other coefficients are assumed to be constant.[10)] At equilibrium state P is given by

$$P = \chi(E - C\theta). \tag{2}$$

Substituting eq. (2) in eq. (1), we obtain

$$F = \frac{1}{2}(a - \chi C^2)\theta^2 + \frac{1}{4}b\theta^4 + C\chi\theta E. \tag{3}$$

Starting with eq. (3), a simple equation for tilt angle θ is obtained by minimizing F with respect to θ:

$$\frac{\partial F}{\partial \theta} = \alpha(T - T_0)\theta + b\theta^3 - C\chi E = 0, \tag{4}$$

where T_0 is given by $T_0 = T_c + \chi C^2/\alpha$ which is a newly defined phase transition temperature. Near T_0 or for large E, θ is simply given as

$$\theta = \left(\frac{C\chi E}{b}\right)^{1/3} \propto E^{1/3}. \tag{5}$$

From the definition of pyroelectric coefficient and eqs. (2) and (4), we can derive

$$\gamma = \frac{dP}{dT} = -\chi C\frac{d\theta}{dT} = \frac{\chi C\alpha\theta}{\alpha(T - T_0) + 3b\theta^2}. \tag{6}$$

The temperature at which γ is maximum can be calculated from the second derivative of eq. (4) with respect to T. Then,

$$\left(\frac{d\gamma}{dT}\right)_{T=T_m} = \frac{-2\gamma(\alpha - 3b\theta\gamma/\chi C)}{\alpha(T - T_0) + 3b\theta^2}. \tag{7}$$

In order for γ to be maximum at T_m, γ has to be zero or $\alpha - 3b\theta\gamma/\chi C = 0$. However, γ is zero only at $T = \infty$ or $T = 0\,\mathrm{K}$. Therefore, the maximum γ is given by

$$\gamma_m = \frac{\chi C\alpha}{3b\theta}. \tag{8}$$

By comparing eq. (8) with eq. (6), we find that the pyroelectric coefficient is maximum at T_0. This indicates that the transition temperature of the second-order phase transition in FLCs can be defined by the temperature at which the pyroelectric coefficient is maximum. The maximum γ depends on the strength of the external field, but phase transition temperature does not change.

Similarly, dielectric constant can be calculated using eqs. (2) and (4) as

*E-mail address: jhkim@hallym.ac.kr

$$\epsilon_0 \Delta\epsilon = \frac{(C\chi)^2}{\alpha(T - T_0) + 3b\theta^2}. \quad (9)$$

The temperature at which the dielectric constant is maximum can be calculated from the second derivative of eq. (10) with respect to T. Then

$$\left(\frac{d\Delta\epsilon^{-1}}{dT}\right)_{T=T_m} = \frac{1}{(C\chi)^2}\left[\alpha - \frac{6\alpha b\theta^2}{\alpha(T - T_0) + 3b\theta^2}\right]. \quad (10)$$

Therefore, T_m satisfies

$$T_m - T_0 = \frac{3b\theta^2}{\alpha}. \quad (11)$$

The dielectric constant is maximum at $T \neq T_0$, which is different from the pyroelectric constant. Since θ is proportional to $E^{1/3}$ near T_0, $(T_m - T_0)$ is proportional to $E^{2/3}$.

To obtain non-chiral Landau coefficients (i.e., α, b, and χC), the pyroelectric coefficient, dielectric constant, and tilt angle are investigated and analyzed using eqs. (6), (8), and (11).

3. Experimental

The FLC materials used in this study were SCE 13 and 854E from the British Drug House. Both materials have the same phase sequences as follows: isotropic → nematic → Sm A → Sm C*. The sample cell was made up of conductive indium–tin–oxide coated glasses which were treated with polyimide. Both glass surfaces of the cell were unidirectionally rubbed so as to provide planar orientation. The cell gap was maintained by glass spacers of 10 μm thick, and the effective electrode area was 0.64 cm^2. The FLCs were filled in the isotropic state, and cooled into the mesophase. Electric contacts were made directly on the internal surfaces of the glasses to apply an external electric field.

We measure the pyroelectric current, capacitance, and tilt angle of the cell simultaneously for the accurate study of phase transition phenomena in FLCs. Figure 1 shows the schematic diagram of the experimental setup. The sample cell was mounted on a hot stage for temperature control, and temperature fluctuations were approximately 5 mK. The hot stage was designed to include a window for thermal heating by a laser beam. The pyroelectric response of each sample was measured using the dynamic Chynoweth technique.[11] A laser diode with a wavelength of 830 nm and an intensity of about 100 mW was used as a light source. The sample cell was periodically heated by a chopped light source. The ac pyroelectric current, generated from the sample during heating, was measured with a lock-in amplifier locked to the reference signal derived from the chopper during the heating or cooling of the hot stage. Due to the collective behavior of LC molecules, it is important to determine the optimized frequency of thermal modulation. In Fig. 2, we present the characteristic curves for the pyroelectric response of 854E at various frequencies. For the measurement, we used a digitizing oscilloscope in conjunction with the current amplifier (Keithley Model 428) in a separate setup. At 10 Hz, the pyroelectric current shows a spike-like response [Fig. 2(a)] due to a longer irradiation sequence than the thermal inertia of the sample. At 100 Hz, the response follows the shape of incident light [Fig. 2(b)]. At a higher frequency (250 Hz), however, the shape is diminished due to the fact that the collective behavior of LC molecules cannot follow the thermal modulation, as shown in Fig. 2(c). Figure 3 shows the frequency dependence of the pyroelectric current of 854E at room temperature. Pyroelectric current increases with increasing the frequency, and an abrupt change was observed with further increase in frequency. From the experiment, we can obtain the best signal-to-noise ratio in 80–130 Hz range. Therefore, we fixed the frequency

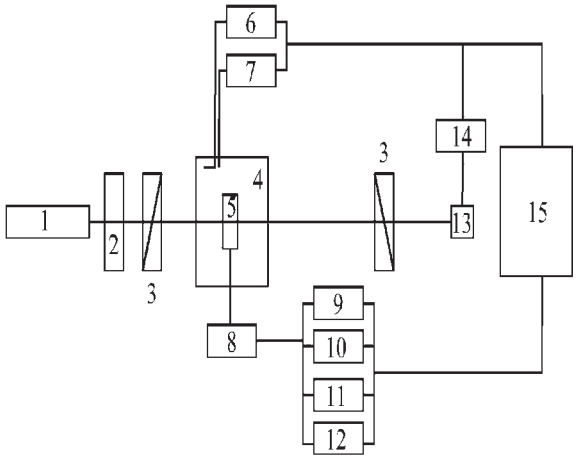

Fig. 1. Schematic diagram of experimental set-up: 1. diode laser, 2. chopper, 3. polarizer, 4. hot stage, 5. sample, 6. DC power supply, 7. digital multi meter, 8. scanner system, 9. lock-in amplifier, 10. LCR meter, 11. DC voltage source, 12. arbitrary waveform generator, 13. detector, 14. oscilloscope, and 15. computer.

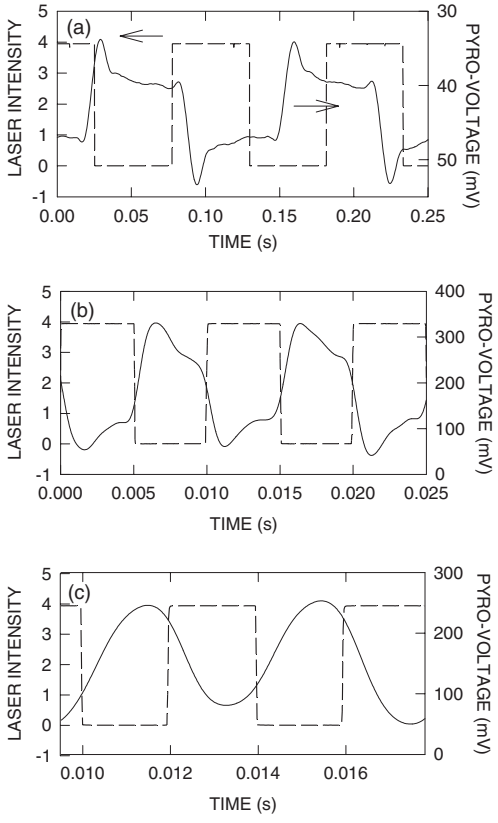

Fig. 2. Pyroelectric response of 854E at various frequencies at room temperature: (a) 10 Hz, (b) 100 Hz, and (c) 250 Hz.

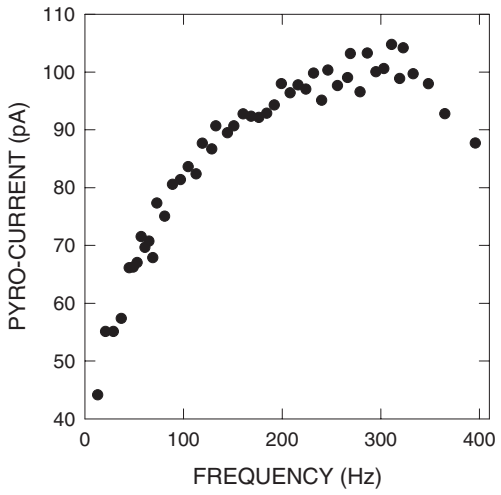

Fig. 3. Pyroelectric current as a function of frequency.

at 100 Hz in succeeding experiments. A detailed description of the dynamic pyroelectric response is published elsewhere.[12,13]

A DC bias was applied using a voltage source (Keithley Model 239). We measured capacitance using an impedance analyzer (HP 4192A) at 1 kHz. Tilt angle was then determined by the measurement of transmittance while applying an AC voltage of 1 kHz. The rubbing axis was rotated 22.5° with respect to the optical axis of the front polarizer. All of these material parameters were measured in order using a high-density switching system (Keithley model 701). Since the measurements were carried out within 5 mK, we can treat the results as though they were measured simultaneously.

4. Results and Discussion

Figure 4(a) shows the pyroelectric current of SCE 13 as a function of temperature for various bias voltages. The pyroelectric current exhibits divergent behavior at the Sm A–Sm C* phase transition temperature at all bias voltages. As we expected in theory, the peak position does not depend on bias voltage, but the magnitude decreases with increasing voltage. Therefore, the Sm A–Sm C* phase transition temperature can be defined by the peak position of pyroelectric current for SCE 13, i.e., $T_0 = 52.34$°C. Note that the peak position shifts to a higher temperature with increasing bias voltage for FLCs with a large EC effect, such as 854E, as shown in Fig. 4(b). In this case, we have to consider a higher order term of θ (i.e., θ^6) in eq. (1) because of the large EC effect of 854E (i.e., tilt angle is about 10° even at $T - T_0 = 1$°C.). Then the temperature for the γ_m is $T_m = T_0 + 5C\theta^4/\alpha$. Therefore, the temperature difference $(T_m - T_0)$ is proportional to $E^{4/3}$. The inset in Fig. 4(b) shows $(T_m - T_0)$ versus $E^{4/3}$. In this study, we restrict our approach to FLCs with a small EC effect such as SCE 13.

In order to calculate pyroelectric coefficient (γ), a calibration procedure must be adopted by measuring spontaneous polarization at a fixed temperature. The measured pyroelectric current $i(\omega)$ is given by

$$i(\omega) = A\frac{dP}{dt} = A\frac{dP}{dT}\frac{dT}{dt} = A\gamma\frac{dT}{dt}, \tag{12}$$

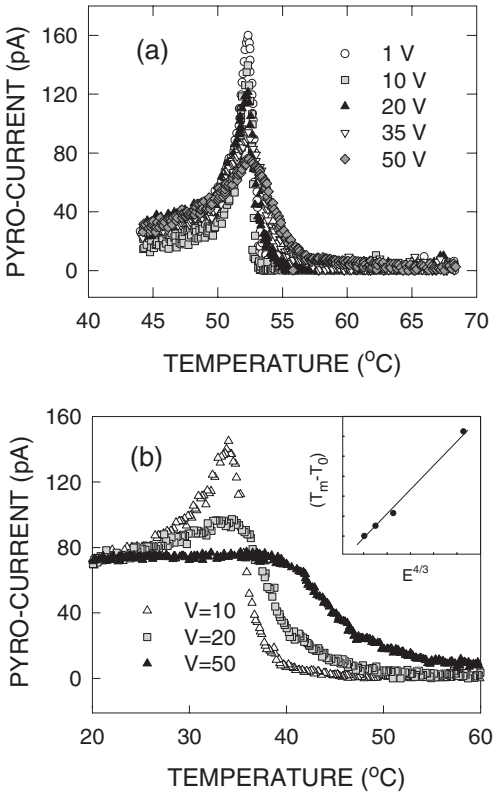

Fig. 4. Pyroelectric currents for (a) SCE 13 and (b) 854E as functions of temperature with various voltages. The inset in (b) is $(T_m - T_0)$ versus $E^{4/3}$.

where A is the area of the electrode, and dT/dt is the rate of heating of the sample which depends on cell geometry, light absorption, and thermal relaxation time of the cell walls. We can calculate polarization at temperature T_1 by integrating of eq. (12) as

$$P(T_1) = \frac{1}{A(dT/dt)}\int_{T_0}^{T_1} i(\omega)dT, \tag{13}$$

where T_0 is the phase transition temperature from the Sm A to Sm C* phases. Figure 5 shows the integration of pyroelectric current for SCE 13 with a bias voltage of 20 V. For SCE 13, the measured P is 20.4 nC/cm^2 at 41°C using the triangular wave method. From the results, we

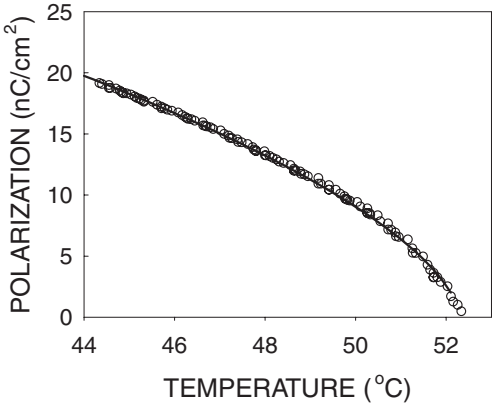

Fig. 5. Integration of pyroelectric current for SCE 13 with bias voltage of 20 V. The solid line is derived from the best fit using $P = P_0(T_0 - T)^\alpha$.

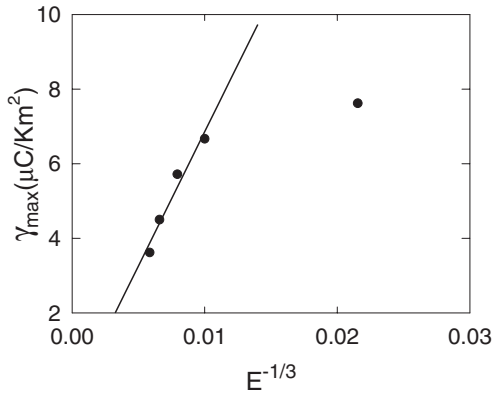

Fig. 6. Maximum pyroelectric coefficient as a function of $E^{-1/3}$. The solid line is derived from the best fit using eq. (8).

found that $A(dT/dt) = 3.2 \times 10^{-3}\,\mathrm{m^2 \cdot {}^\circ K/s}$.

In Fig. 6, we plot the maximum pyroelectric coefficient (γ_m) for SCE 13 as a function of $E^{-1/3}$, which shows linear dependence except in the low-field regime. Since the pyroelectric coefficient diverges at paraelectric (Sm A)-ferroelectric (Sm C*) phase transition temperature, we can expect that a higher γ_m even at a low bias voltage in more precise temperature scan. The solid line in Fig. 6 is derived from the best fit obtained using eq. (3) with $\theta \approx (\chi CE/b)^{1/3}$. Except at a low-field strength, the equation provides a satisfactory agreement with a proportional coefficient of $(7.19 \pm 1.06) \times 10^{-3}$ in mks unit.

In Fig. 7(a), we present the capacitance of SCE 13 as a function of temperature with various bias voltages. The magnitude and peak position of capacitance change with different bias voltages. Particularly, the peak position shifts to higher temperature with increasing bias voltage. The differences between peak positions in pyroelectric current and capacitance are shown in Fig. 7(b) as a function of $E^{2/3}$. As we described in theory, it is linearly proportional to $E^{2/3}$. The solid line in the figure represents the best fit to the experimental results according to eq. (7) with a proportional coefficient of $(1.53 \pm 0.07) \times 10^{-4}$ in mks unit.

For a small tilt angle, the temperature gradient of tilt angle $d\theta/dT$ is linearly proportional to γ, as shown in eq. (3) with a proportional coefficient of χC. Fig. 8 shows γ as a function of $d\theta/dT$. The solid line in the figure is the result of the best fit with $\chi C = (1.02 \pm 0.10) \times 10^{-3}\,\mathrm{FV/m}$. Using the values from three simple linear fittings, we can calculate the non-chiral coefficients of Landau expansions. In Table I, we summarize the values from our experiment and compare them with other experimental results. The values of α and

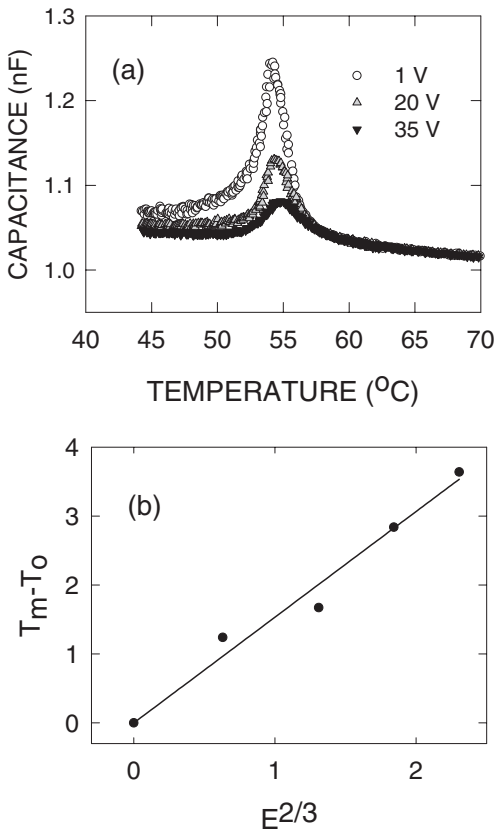

Fig. 7. (a) Capacitance as a function of temperature with various bias voltages. (b) Difference in peak position between pyroelectric and capacitance measurements. The solid line in (b) is derived from the best fit using eq. (12).

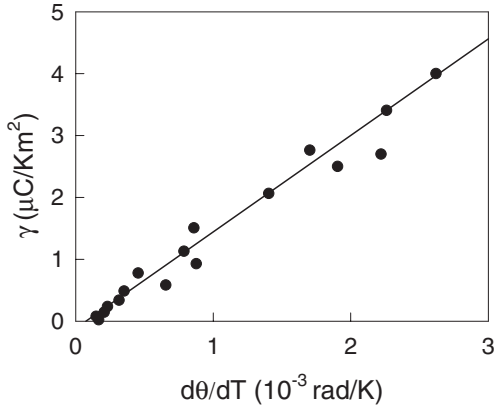

Fig. 8. Temperature gradient of θ as a function of γ at 20 V. The solid line is derived from the best fit using eq. (6).

Table I. Summary of determined non-chiral Landau coefficients.

Authors	LC	α (10^3 J/Km^3)	b (10^4 J/m^3)	$C\chi$ (10^{-3} FV/m)
Carlsson and Dahl[4]	DOBAMBC	50	8.50	1.17
Huang and Dumrongrattana[6]	DOBAMBC	22.6	26	0.73
Bahr *et al.*[7]	LC-7	89	−8.5	3.40
Lee and Patel[8]	764E	20	170	3.80
Giëbetaelmann and Zugenmaier[9]	FLC6430	26.5	6.69	1.08
This work	SCE 13	17.8	74.8	1.02

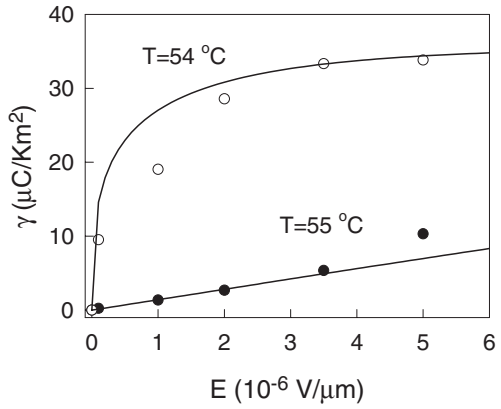

Fig. 9. Measured and calculated γ values as functions of field strength. In the calculation, we use eq. (6) with Landau coefficients in Table I.

χC obtained in this experiment are in the same order of magnitude as those of other results. However, the value of b in 764E and our sample is more than 10 times larger than that of other compounds. This large b value supports that Sm A–Sm C* transitions of 764E and SCE 13 are strong second-order phase transitions. A relatively small χC with respect to 764E indicates a relatively small EC effect of SCE 13.

In order to check the validity of the parameters obtained, we calculate the pyroelectric coefficient as a function of field strength using eq. (3) with the calculated Landau coefficients in Table I. In the calculation, we assume that θ is linearly proportional to E at 55°C but shows nonlinear behavior at 54°C. In Fig. 9, symbols and solid lines are the measured pyroelectric coefficient and calculated values, respectively. We found that the calculated value provides an excellent description of pyroelectric behavior as a function of field strength. This confirms that the Landau coefficients derived from our experiment satisfactorily describe the Sm A–Sm C* phase transition of SCE 13.

5. Conclusions

We studied the Sm A–Sm C* phase transition of SCE 13 by the simultaneous measurements of tilt angle, dielectric constant, and pyroelectric coefficient as functions of temperature with various bias voltages. The pyroelectric coefficients are maximum at the phase transition temperature, and the temperature does not depend on the applied voltage. However, the temperature for the maximum dielectric constant slightly increases with increasing applied voltage. The simple linear fits of the Landau model to the experimental results provide mean-field coefficients, which agree well with those of other experiments.

Acknowledgements

This work was supported by the Hallym Academy of Sciences, Hallym University, Korea, 2001.

1) R. B. Meyer, L. Liebert, L. Strzelecki and P. Keller: J. Phys. Lett. (Paris) **36** (1975) 69.
2) N. A. Clark and S. T. Lagerwall: Appl. Phys. Lett. **36** (1980) 899.
3) J. W. Goodby *et al.*: *Ferroelectric Liquid Crystals: Principles, Properties, and Applications* (Gordon and Breach, Philadelphia, 1991).
4) T. Carlsson and I. Dahl: Mol. Cryst. Liq. Cryst. **95** (1983) 373.
5) S. Dumrongrattana, C. C. Huang, G. Nounesis, S. C. Lieu and J. M. Viner: Phys. Rev. A **34** (1986) 5010.
6) C. C. Huang and S. Dumrongrattana: Phys. Rev. A **34** (1986) 5020.
7) C. Bahr, G. Heppke and B. Sabaschus: Ferroelectrics **84** (1988) 103.
8) S.-D. Lee and J. S. Patel: Appl. Phys. Lett. **54** (1988) 1653.
9) F. Giebelmann and P. Zugenmaier: Phys. Rev. E **52** (1995) 1762.
10) I. Muševič, R. Blinc and B. Žekš: *The Physics of Ferroelectric and Antiferroelectric Liquid Crystals* (World Scientific, Singapore, 2000).
11) A. G. Chynoweth: J. Appl. Phys. **27** (1956) 78.
12) Y. Kim, J.-H. Kim, S.-D, Lee and G. Park: Ferroelectrics **156** (1994) 197.
13) C.-J. Yu, J.-H. Lee, J.-H. Kim and S.-D. Lee: J. Kor. Phys. Soc. **32** (1998) s1066.